Brownian Dynamics Simulation of Transport Properties in Potassium Ion Channels

S. Aboud*, D. Marreiro**, M. Saraniti** and R. Eisenberg*

*Molecular Biophysics Department,Rush University,Chicago, IL, USA
**Electrical and Computer Engineering Department,
Illinois institute of Technology, Chicago, IL, USA

ABSTRACT

In this work, a self-consistent Langevin dynamics-Poisson solver (LDPS) is used to model the ionic transport properties in ion channel systems. The charge transport behavior in the bulk electrolyte has been compared with the results of an analytic model. Within the LDPS framework, the molecular structure of both the protein and the lipid bilayer are explicitly accounted for, and the atomistic representation of the channel is embedded in the molecular structure of a patch of membrane, included in the computational domain.

Keywords: Brownian Dynamics, Langevin, Poisson equation, potassium channels, electrolyte solution

1 Introduction

Potassium (K) channels are a large class of transmembrane proteins that are probably present in all cells [1], and play a crucial role in stabilizing the membrane potential in excitable cells. They are characterized by an extreme selectivity (their permeability for K^+ is about 10^3 times larger than for the smaller Na^+ ions), and by a high diffusivity (comparable to bulk water).

The molecular structure of several K channels has been recently disclosed by means of X-ray spectroscopy. In particular, a 3.3 Å resolution mapping of the ligand-gated bacterial MthK channel structure, which opens in response to intracellular Ca^{2+}, has been successively disclosed by [2].

In this work, a Brownian dynamics simulator based on the self-consistent coupling of the Langevin equation with the P^3M force field scheme [3] [4], is used to model ionic transport. Within this approach, the molecular structure of both the protein and lipid bilayer are explicitly accounted for. Indeed, an atomistic representation of the channel is embedded in the molecular structure of a patch of membrane, and is included in the computational domain as described in [5] [6].

In the following section of this paper, the implementation of the LDPS simulation tool is discussed. In particular, the discretization scheme chosen for the numeric solution of the Langevin equation is presented along with the impact of the integration timestep on the simulated ionic dynamics. A calibration procedure for the bulk electrolyte solution is then presented and comparisons are made with the solution of an analytic integral expression. The implementation of the molecular structure of the lipid membrane and potassium channel protein is then described and the electrostatic behavior of the channel pore is shown. A discussion is carried out of the impact of the short-range field schemes on the simulated ion dynamics. Finally, the limitations of the Brownian dynamics approach will be discussed within the ion channel simulation framework.

2 Langevin Dynamics-Poisson Solver

The full Langevin equation is,

$$m_i \frac{d\mathbf{v}_i(t)}{dt} = -m_i\gamma\mathbf{v}_i(t) + \mathbf{F}_i(\mathbf{r}_i(t)) + \mathbf{R}_i(t) \quad (1)$$

where m_i is the mass of the ith particle, and $\mathbf{v}_i$ is its velocity at time t, γ is the friction coefficient, $\mathbf{F}_i$ is the force on the particle i due to the presence of all other particles in the system and any external boundary conditions, including dielectric boundaries, and $\mathbf{R}_i$ is a fluctuating force due to the molecular bombardment of water on the ions, and is treated as a Markovian random variable with zero mean.

A third order algorithm is used for the calculation of the Brownian particle trajectories [7]. Within this approach the force is expanded in a power series,

$$F(t) \sim F(t_n) + \dot{F}(t_n)(t - t_n), \quad (2)$$

where $\dot{F}$ denotes the time derivative, and is substituted back into Eq. 1, resulting in the following solution of the Langevin equation,

$$v(t) = v(t_n)e^{-\gamma\Delta t} + (m\gamma)^{-1}F(t_n)(1 - e^{-\gamma\Delta t}) \quad (3)$$

$$+ (m\gamma^2)^{-1}\dot{F}(t_n)(\gamma\Delta t - (1 - e^{-\gamma\Delta t})) \quad (4)$$

$$+ (m)^{-1}e^{-\gamma\Delta t}\int_{t_n}^{t} e^{-\gamma(t'-t_n)}R(t')dt', \quad (5)$$

where $\Delta t = t_n - t$. The ionic positions are then calculated with the expression,

$$x(t_{n+1}) = 2x(t_n) - x(t_{n-1})e^{-\gamma(t_n - t_{n-1})} \quad (6)$$

$$+ \int_{t_n}^{t_{n+1}} v(t')dt' + e^{-\gamma(t_n - t_{n-1})}\int_{t_{n-1}}^{t_n} v(t')dt'. \quad (7)$$

The result is a set of equations for the particle trajectories that are dependent on a bivariant gaussian distribution, and which reduce to the Verlet [8] algorithm in the limit that the friction coefficient goes to zero. Because of this integration approach the timestep is not limited by the velocity relaxation time (i.e. the reciprical of the friction coefficient), and a long timestep (∼20 fs) can be used.

A Poisson P^{3}M algorithm [4] is implemented to resolve the electrostatic force fields. The long range interaction, which includes the external boundary conditions and the dielectric boundary interfaces is resolved with a multigrid [9] Poisson solver [10]. A nearest grid point scheme [3] is used for the charge assignment and force interpolation. The short range interaction for close particles is modeled with a Coulomb term and a van der Waals function which is either a Lennard-Jones [11] or and inverse power expression [12]. The short range Lennard-Jones potential between two particles is,

$$u(r_{ij}) = 4\epsilon \left[\left(\frac{\sigma}{r_{ij}} \right)^{12} - \left(\frac{\sigma}{r_{ij}} \right)^{6} \right] + \frac{q_i q_j}{4\pi\epsilon_r r_{ij}} \qquad (8)$$

where σ and ϵ represent the zero of the the potential and the depth of the potential well, respectively, q_i is the charge of the ith particle and ϵ_r is the bulk dielectric constant. Another form of the short-range potential which can be used is,

$$u(r_{ij}) = \frac{\beta_{ij} \left| q_i q_j \right|}{4\pi\epsilon r_{ij}(p+1)} \left(\frac{s_i + s_j}{r_{ij}} \right)^{p} + \frac{q_i q_j}{4\pi\epsilon_r r_{ij}}, \qquad (9)$$

where β_{ij} is an adjustable parameter, s_i is the size of the ith particle, and p is the hardness of the particle. A comparison of these two potentials is shown in Fig. 1, for β=1.

3 Bulk Electrolyte Solution

Several measurements are made to calibrate the proposed Brownian simulation approach for bulk electrolyte solutions. The simulation domain used is a homogeneous 20x20x20 tensor-product grid with mesh spacing 0.5 nm in all three directions. In this work, Dirichlet boundary conditions have been placed on opposite planes of the 3D volume, while Neumann conditions are imposed on the other 4 planes. Ions are specularly reflected from the Neumann boundaries, while the Dirichlet "electrodes" are treated as open boundaries and ions which traverse these regions exit from the simulation. In order to maintain the ion concentration ions must therefore be injected into the simulated volume. The computational domain is assumed to represent a small portion of a quasi-infinite electrolyte bath and the total molar concentration in the Dirichelt "electrodes" is conserved at each time step. The velocity of the injected ions is

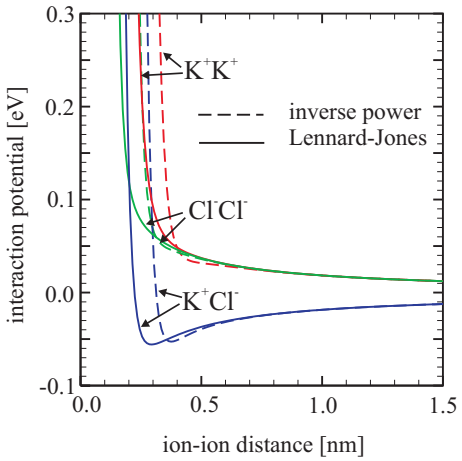

Figure 1: Comparison of short range Lennard-Jones and inverse power potential for K+ and Cl- in an aqueous solution.

calculated according to a Maxwell distribution in the directions parallel to the contacts and a half-Maxwellian in the normal direction.

As an initial test, the radial distribution function (RDF) of the electrolyte solution is calculated. The RDF is a measure of the liquid structure and is of central importance because it can be used to obtain a complete description of the thermodynamic state of the system [13]. To validate the approach, comparisons are made with the solution of the Ornstein-Zernike equation [13] which is combined with the closure relation given by the hypernetted chain approximation (HNC) [14]. The Ornstein-Zernike equation for a mixture is [13],

$$h_{ij}(r_{12}) = c_{ij}(r_{12}) + \sum_l \rho_l \int h_{il}(r_{13}) c_{lj}(r_{23}) dr_3, \qquad (10)$$

where the RDF is $g_{ij}(r_{12}) = h_{ij}(r_{12}) + 1$, and h_{ij} is a measure of the total influence of particle 1 on particle 2 at a distance r_{12}. The direct correlation between particle 1 and particle 2 is expressed with $c_{ij}(r_{12})$ and ρ_l is the density of species l. To obtain the HNC closure relation, the direct correlation function is written as the difference between the total radial distribution and the radial distribution without any direct interactions included:

$$c(r) = e^{\beta w(r)} - e^{\beta[w(r)-u(r)]} \sim e^{\beta w(r)} - 1 + \beta[w(r) - u(r)], \qquad (11)$$

where the total particle interaction is $w(r)$, $u(r)$ is the direct particle-particle interaction, and β is the thermal voltage $1/k_B T$. The radial distribution function is then calculated by iterating the following set of equations as

suggested by [15],

$$\hat{y}(q) = \hat{c}(q)/(1 - \rho\hat{c}(q)) - \hat{c}(q) \quad (12)$$

$$g(r) = exp[y(r) - u(r)] \quad (13)$$

$$c(r) = g(r) - 1 - y(r) \quad (14)$$

where $\hat{f}(q)$ denotes the three dimensional Fourier transform of $f(r)$ and

$$y(r) = e^{\beta u(r)} g(r). \quad (15)$$

The RDF corresponding to aqueous KCl at a 150 mM concentration is shown in Fig. 2 for the analytic HNC approach and the LDPS. Both LDPS and HNC use the Lennard-Jones potential, with parameters taken from [16], and the integration timestep of the LDPS is 5 fs. Results show good agreement, although the peak is lower in the LDPS for the K^+Cl^- RDF. This may be due to spurious fluctuations of the ionic population present at low ion concentration. The impact of higher order charge assignment schemes in the Poisson solver is also being investigate.

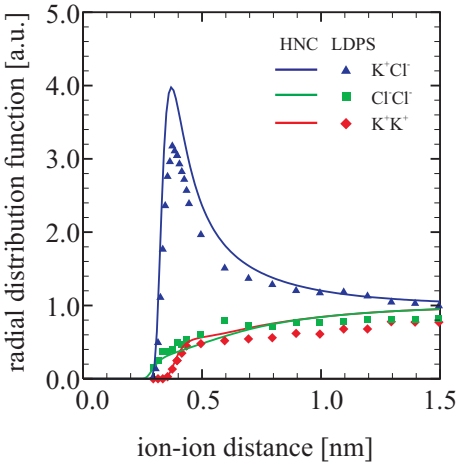

Figure 2: Radial distribution function in aqueous KCl at 298 K at a concentration of 150 mM calculated with HNC and LDPS

The equivalent conductivity for several aqueous KCl solutions under nonequilibrium conditions is also calculated with very good agreement with experimental values [6] [17], for several molar concentrations. The calculted conductivity tends to deviate from the experiemental values at molar concentrations higher than approximately 0.5 molar. This is due to an expected break-down in the validity of the primitive water model, occuring when the average distance between ions becomes comparable to the diameter of water.

4 Ion Channel Simulation

To include the channel protein and lipid membrane in the computational domain, the atomic coordinates and charge distributions are inserted explicitly using a combination of experimental data and simulation result, as explained in [6]. The atomic coordinates of the Mthk ion channel structure is obtained from X-ray diffraction experiments of crystallized proteins [2]. An energy minimization based approach [5] is applied to insert the channel into the interior of a phospholipid membrane, initially modelled with a molecular dynamics simulation [18]. A plot of the MthK K+ channel inserted into the lipid bilayer is shown in Fig. 3.

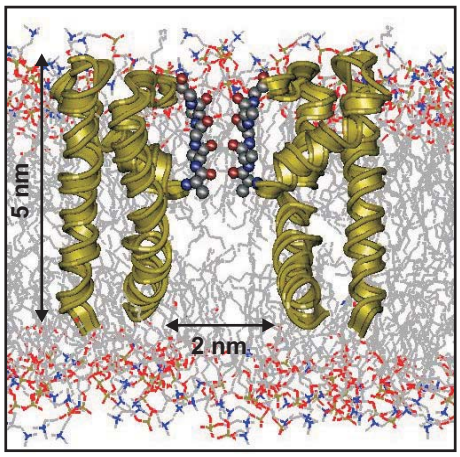

Figure 3: Two sides of the MthK K+ channel structure embedded in an explicit lipid bilayer.

Within the P^3M approach used for the force field calculation, the short-range component of the force, including both the Coulomb interaction and finite-size effects of the ions, is implemented by using a Lennard-Jones or an inverse power relation [3]. When applied to simple bulk solutions, this representation produces values for the equivalent conductivity that are in good agreement with experiment. However, the nature of the short-range interaction inside the ion channel is more complicated to model. As an initial probe into the electrostatic behavior of the channel pore, a test point charge is placed at various locations and the total force on the particle is calculated. This force is then integrated to obtain the potential profile along the channel. The potential profile is also calculted when a K+ ion is inserted in the center of the MthK channel, to investigate the effect of the short-range interaction. The short-range potential is given by the inverse power relation of Eq. 9. A comparison of the resulting potential profiles, both without the finite-size effects and with the short-range described by the inverse power relation are shown in Fig. 4. As can be seen, the inclusion of the finite size effect of the ion results in an increase of the electrostatic features due to the positions of the atoms in the selectivity filter. In addition the use of a non-homogeneous dielectric constant within the channel pore further alters

the electrostatic profile.

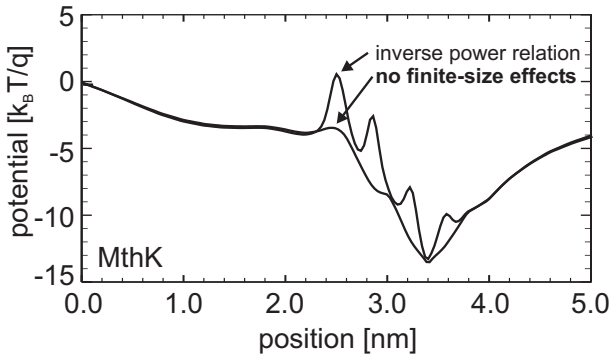

Figure 4: A comparison of the electrostatic potential acting on a K+ ion as a function of position along the center of the MthK channel for a short-range interaction that is based on an inverse power relation and when finite-size effects are neglected.

The atomic coordinates of both the protein and lipid bilayer have been treated as static quantities in this work. In reality, the motion can be significant and the result can drastically alter the shape of the potential, particularly in the selectivity filter. This motion must be accounted for in order to accurately describe the ionic transport. Further work needs to be done to investigate the influence of the motion of atoms on the electrostatic characteristics, as well as the correct form of the short-range electrostatic interaction within the cavity. Another important element of the simulation domain which must be included is a more accurate representation of the water inside the channel.

5 Conclusion and Discussion

The self-consistent LDPS has been used to model the transport behavior in ion channel systems. The first step is to calibrate the simulation approach for the bulk electrolyte solutions. An analytic integral equation describing the RDF was calclate with the HNC closure relation to validate the results of the LDPS in the equilibrium regime. The results show good agreement, although the LDPS peak is slightly lower. This may be due to fluctuations resulting from the sparsity of the ionic population.

To simulate the ion channel and lipid membrane system, their atomic coordinates and charge distribution have been explicately inserted in the compuational domain. Preliminary results of the distribution of the electrostatic potential along the channel show expected behavior, and demonstrate the sensitivity of the forces on both the short range interactions and the dielectric properties of the channel.

Acknowledgement

This work was supported in part by the grant T32 HL07692 of the National Institute of Health.

REFERENCES

[1] B. Hille, *Ionic Channels of Excitables Membranes*, Sinauer, Massachusetts, 1992.

[2] Y. Jiang, A. Lee, J. Chen, M. Cadene, B.T. Chait, and R. MacKinnon *Nature*, vol. 417, pp. 515–522, May 2002.

[3] R.W. Hockney and J.W. Eastwood, *Computer Simulation Using Particles*, Adam Hilger, Bristol, 1988.

[4] C.J. Wordelman and U. Ravaioli *IEEE Transaction on Electron Devices*, vol. 47, no. 2, pp. 410–416, Feb 2000.

[5] J.D.Faraldo-Gomez, G.R.Smith, and M. S. P. Sansom vol. 31, pp. 217–27, European Biophysics Journal.

[6] S. Aboud, M. Saraniti, and R. Eisenberg *Journal of Computational Electronics*, 2004, to be published.

[7] W.F. van Gunsteren and H.J.C. Berendsen *Molecular Physics*, vol. 45, no. 3, pp. 637–647, 1982.

[8] L. Verlet *Physical Review*, vol. 159, no. 1, pp. 159–103, July 1967.

[9] W. Hackbush, *Multi-Grid Methods and Applications*, Springer–Verlag, Berlin, 1985.

[10] S.J. Wigger, M. Saraniti, and S.M. Goodnick in *Proceedings of Second International Conference on Modeling and Simulation of Microsystems, MSM99*, Puerto Rico (PR), April 1999, pp. 415–418.

[11] R. Stephen Berry, Stuart Alan Rice, and John Ross, *Physical Chemistry*, Oxford University Press, II edition, May 2000.

[12] P. Turq, F. Lantelme, and H.L. Friedman *The Journal of Chemical Physics*, vol. 66, no. 7, pp. 3039–3044, April 1977.

[13] D.A. McQuarrie, *Statistical Mechanics*, University Science Books, Sausalito, CA, 2000.

[14] J. Barthel, H. Krienke, and W. Kunz, *Physical Chemistry of Electrolyte Solutions*, Springer, 1998.

[15] K.-C. Ng *Journal of Chemical Physics*, vol. 61, pp. 2680–2689, 1974.

[16] Wonpil Im, Stefan Seefeld, and Benoit Roux *Biophys. J.*, vol. 79, no. 2, pp. 788–801, 2000.

[17] V. M. M. Lobo, *Electrolyte solutions: literature data on thermodynamic and transport properties*, vol. 2, Coimbra, 1975.

[18] D. Peter Tieleman, Mark S. P. Sansom, and Herman J. C. Berendsen *Biophys. J.*, vol. 76, no. 1, pp. 40–49, 1999.